We are IntechOpen, the world's leading publisher of Open Access books
Built by scientists, for scientists

6,900
Open access books available

185,000
International authors and editors

200M
Downloads

154
Countries delivered to

Our authors are among the

TOP 1%
most cited scientists

12.2%
Contributors from top 500 universities

BOOK CITATION INDEX
CLARIVATE ANALYTICS
INDEXED

WEB OF SCIENCE™

Selection of our books indexed in the Book Citation Index
in Web of Science™ Core Collection (BKCI)

Interested in publishing with us?
Contact book.department@intechopen.com

Numbers displayed above are based on latest data collected.
For more information visit www.intechopen.com

Adaptive Control for Estimating Insulation Resistance of High-Voltage Battery System in Electric Vehicles

Yi-Hsien Chiang and Wu-Yang Sean

Additional information is available at the end of the chapter

Abstract

To ensure electrical safety and reliability in electric vehicles equipped with a high-voltage battery pack, an insulation monitoring circuit is indispensable to continuously monitor the insulation resistance during charging or driving. Existing methods such as injecting specific signals into the monitoring circuit and earth help to extract the resistance value from the voltage waveform. However, parasitic or stray capacitances in the monitoring circuit, which might introduce higher order dynamics into the waveform, are ignored. To avoid estimation error, the insulation resistance must be known in advance to carry out parameter calibration. In this chapter, one parasitic capacitance is applied in the circuit model and a new adaptive algorithm based on Lyapunov stability is employed to estimate the insulation resistance. This new online monitoring method and circuit are verified through simulation and experimentation, respectively. The results demonstrate that the proposed method can quickly react and track variations of insulation resistance on both positive and negative direct current (DC) lines.

Keywords: insulation resistance, adaptive control, electric vehicle, high-voltage battery system, reliability

1. Introduction

For improving efficiency, an increasing number of devices are operated at high-voltage levels to reduce losses in power transmission and power conversion. In the case of energy and power systems for electrical vehicles (EVs), a high-efficiency electrical device can be achieved using a high-voltage design. State-of-charge (SoC) and state-of-health (SoH) define the capability and reliability of a high-voltage battery, respectively. To determine these two parameters instantaneously, it is required to develop a simple, training-free, and easily implemented scheme.

Based on an equivalent-circuit model (ECM), the electrical performance of a battery can be formulated into a state-space representation. Besides, underdetermined model parameters can be arranged linearly so that an adaptive control approach can be applied [1]. However, electric shock may be harmful to passengers if insulation failure occurs. As insulation resistance in EVs varies with the operation environment and the reliability of the dielectric material [2], an online insulation-fault detection method is required to ensure that the insulation resistance stays within safe limits before startup or during the operation of high-voltage systems.

To ensure electrical safety in high insulation resistance, insulation inspection technologies have been widely applied in distribution networks [3–5] and EVs [6–13]. To analyze the dynamic insulation signals, the monitoring circuit is conventionally modeled by using two individual resistors connected with a DC high-voltage line to the earth ground. The basic concept used in estimating these two resistance values is to connect an additional circuit bridge composed of resistors and switches to obtain the differential current loops and corresponding voltages [8–11], but the resistance can only be measured if no current is conducted. As a result, these methods are barely suitable even for offline detection. A more practical approach for online detection is to continuously inject an excitation pulse signal into the negative terminal through a capacitor. The insulation resistance value can be acquired by analyzing the time-constant or the amplitude of the voltage waveform [12, 13]. However, parasitic or stray capacitance generally occurs in insulation loops, and causes considerable estimation error if they are ignored in the circuit model. In this chapter, we employ one typical capacitance in the monitoring circuit and propose a new adaptive algorithm for estimating both the resistance and capacitance values.

2. Topology of insulation monitoring circuit

To follow the process illustrated by Sottile and Tripathi [14], the high-voltage system we consider in this chapter could be an EV driving system that is powered by a high-voltage battery or a UPS that stores electricity to provide emergency power. As illustrated in **Figure 1**, a high-voltage system consists of a high-voltage battery pack, an inverter, a converter, an AC load, and an AC source. The DC sides of the inverter and converter are connected in parallel with the high-voltage battery pack. The AC side of the inverter is connected to a two-phase or three-phase load. In other cases, the AC side of the converter could be connected to a two-phase or three-phase source. Here, to consider an EV power system, we assume the AC load to be a traction motor driven by an inverter, with the converter acting as a charger that converts AC power from the grid or generator to DC power for charging the battery pack. In a UPS or a renewable energy system, however, both the AC load and source have the same grid network. Moreover, the inverter must be properly controlled to deliver power in phase with the grid power waveform.

The DC power line of the circuit connected to the high-voltage system is electrically isolated from the enclosure, i.e., the ground or chassis. Thus, we can determine the insulation status by measuring or estimating the resistance between the node on the positive-voltage line (+) or
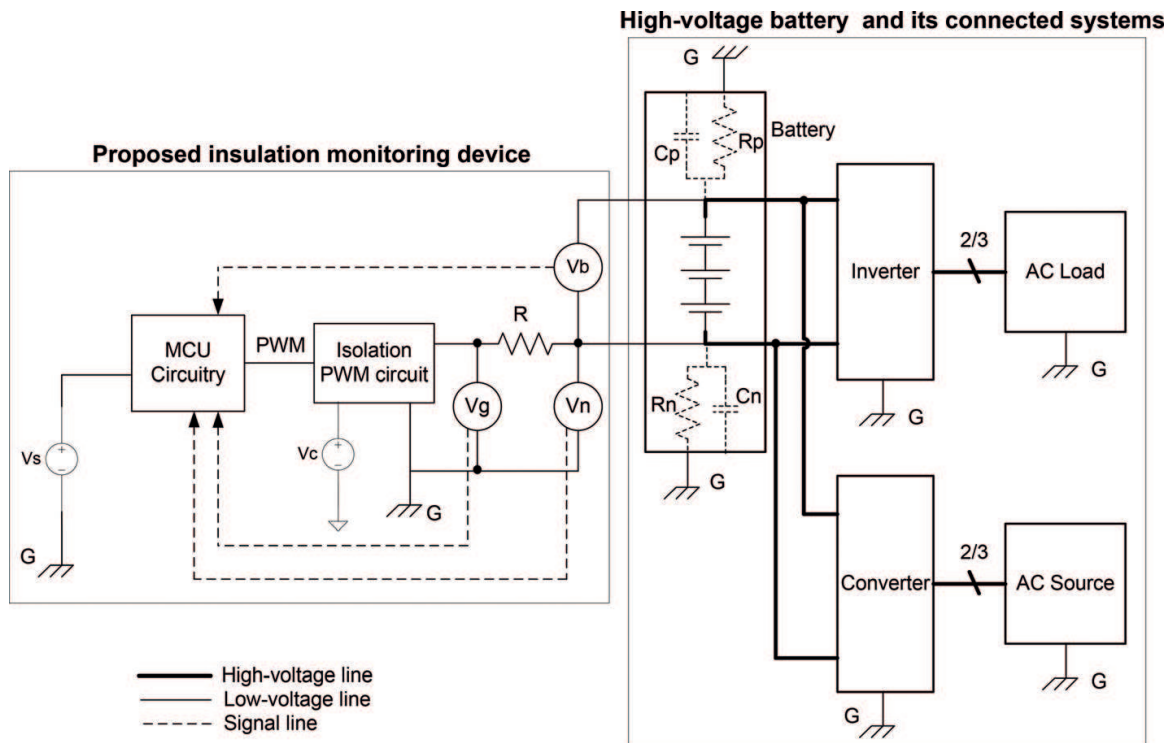
Figure 1. Proposed insulation monitoring circuit.

negative-voltage line (−) and the node with the equivalent electric potential to the ground. The electrical insulation in such a high-voltage system can be simply modeled by a resistor and a stray capacitor in a parallel connection, as shown in **Figure 1**, where R_p/R_n and C_p/C_n denote the positive/negative-line resistance and capacitance of the high-voltage system, respectively. We note that stray capacitance, which has been essentially ignored in previous studies, may yield considerable error in the RC circuit of the voltage waveform. In this work, we consider this higher-order dynamic response in our estimation model, and thus expect a more accurate result. To address this situation, our proposed insulation monitoring circuit, powered by the low-voltage battery V_s, has two outputs that are connected to the positive and negative nodes of the high-voltage system, as shown in **Figure 1**. In the monitoring circuit, we programmed an MCU (micro-control unit) to generate a PWM (pulse-width modulation) signal with a random duty-width sequence $d(t)$, which can be obtained by the PRBS (pseudo random binary sequence) method, which is widely used in systematic identification processes to fully excite the system dynamics. One example of a PWM signal is that shown in **Figure 2**, where $d(t)$ denotes the time-varying duty of the PWM, T is the time period, and $V_w(t)$ is the PWM output with ON and OFF voltage levels. The isolated PWM circuit generates random magnitude voltages in response to the random duty cycle sent from the MCU. Several topologies can achieve isolation and multiple-voltage generation on demand. For example, a photo-coupler provides electrical isolation and regulates the time for charging the output capacitor Cf, as illustrated in **Figure 3(a)**. We use the diode D_1 between the Rf and the external R to prevent any indirect connection to the ground via the Rf when the photo-coupler is turned ON. More specifically, we impose an R + Rf insulation resistance for the system when the coupler is
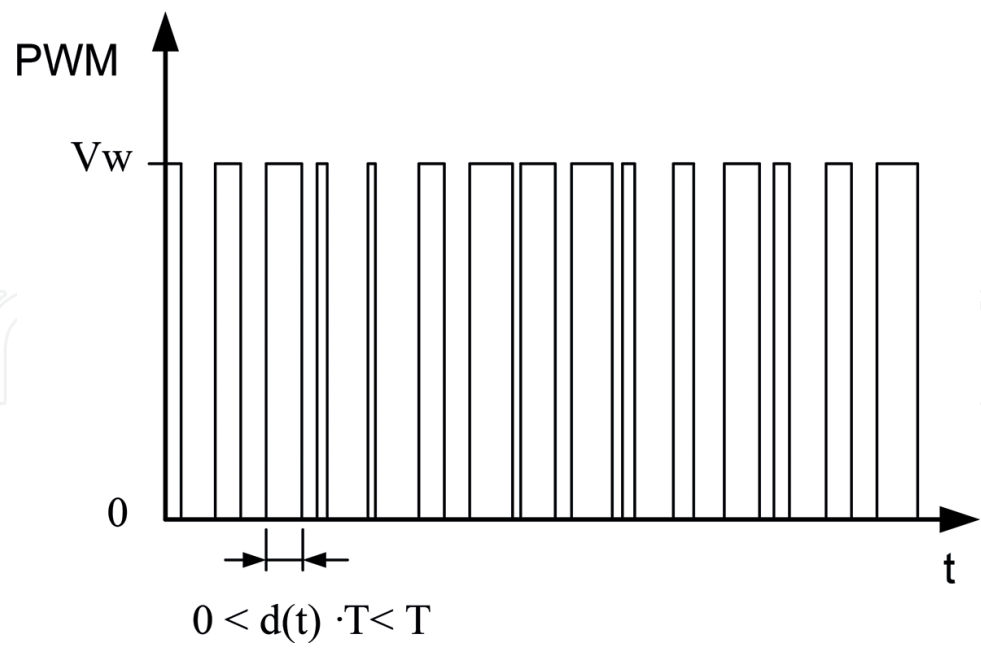
Figure 2. PWM signal generated using the PRBS method. (a) Photo-coupler circuit for electrical isolation and multiple-voltage generation. (b) General topology of the isolated DC/DC converter.
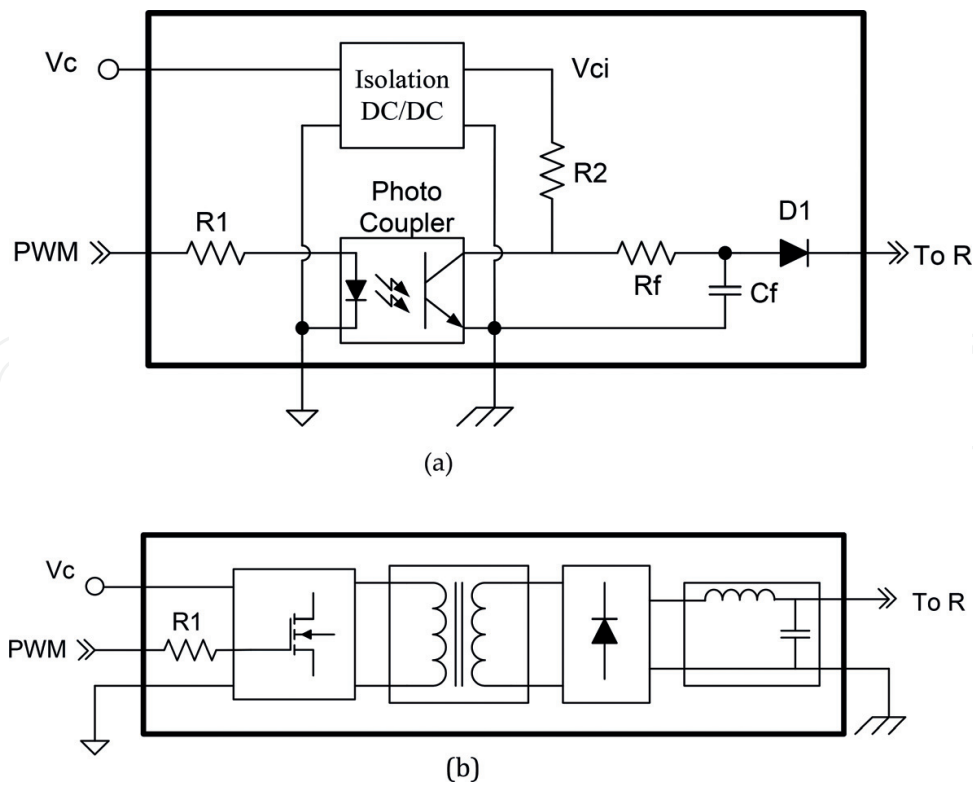

Figure 3. Several topologies for implementing the proposed isolation circuit.

turned ON, without diode D1 as a barrier. The other feasible topology is to isolate the DC/DC converter, such as a forward converter, a fly back converter, or a push–pull converter, as shown in **Figure 3(b)**. With this method, V_c is a DC source that can be generated from the external low-voltage source V_s. Then, the random voltage signal passes through a resistor R and is injected into a node on the negative line of the DC link. Three voltage measurements are required in this method, as shown in **Figure 1**. V_b is the voltage of the high-voltage system. V_n is the voltage between the high-voltage negative terminal and the ground, and V_g is the output voltage of the isolation circuit. The MCU continuously reads the instantaneously measured voltage for the online estimation of the insulation resistance R_p as well as R_n, using the derived adaptive control algorithm.

3. Equivalent circuit model

This high-voltage system connected to the insulation monitoring circuit can be modeled as an equivalent circuit, as illustrated in **Figure 4**, where V_b is the voltage of the high-voltage battery pack, V_a is the voltage of the two- or three-phase AC source or AC machine, the inverter/converter block is the power electronic circuit used to convert power between the AC and DC power stages, and V_g is the output voltage of the isolation circuit. R_p/R_n is the insulation resistor between the ground and the positive/negative terminal of the high-voltage battery pack. C_p and C_n are stray capacitors connected in parallel with R_p and R_n, respectively. Resistor R, which connects the positive terminal of the random voltage sources V_g and the negative terminal of the battery voltage V_b, forms a closed loop between the monitoring circuit and the high-voltage system. We note that the battery voltage V_b, the ground G, and the other insulation resistors and parallel capacitors form the other loop in the circuit.

Therefore, we estimate the insulation resistances R_n and R_p online by an algorithm that is based on the adaptive control law. According to Kirchhoff's circuit laws, the equivalent circuit shown in **Figure 4** can be described as follows:
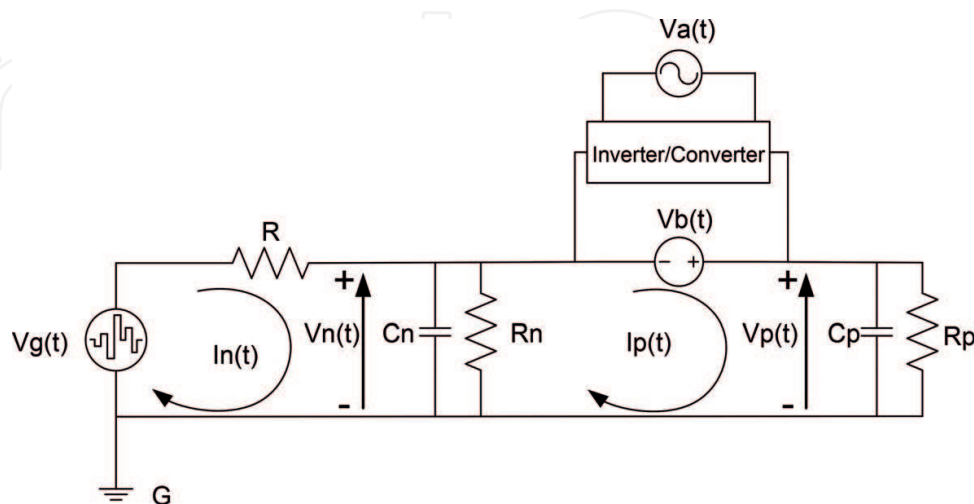

Figure 4. Equivalent circuit model for the insulation monitoring system.

$$I_P = C_P \dot{V}_P + \frac{V_P}{R_P} \tag{1}$$

$$I_N - I_P = C_N \dot{V}_N + \frac{V_N}{R_N} \tag{2}$$

Substituting Eq. (1) into Eq. (2), together with

$$V_P = V_B + V_N,$$

yields:

$$
\begin{aligned}
I_N &= C_N \dot{V}_N + \frac{V_N}{R_N} + I_P \\
&= C_N \dot{V}_N + \frac{V_N}{R_N} + C_P \dot{V}_P + \frac{V_P}{R_P} \\
&= C_N \dot{V}_N + \frac{V_N}{R_N} + \frac{V_P}{R_P} + C_P(\dot{V}_B + \dot{V}_N) \\
&= (C_N + C_P)\dot{V}_N + C_P \dot{V}_B + \frac{V_N}{R_N} + \frac{V_P}{R_P},
\end{aligned}
$$

which can be rewritten as follows:

$$
\begin{aligned}
\dot{V}_N &= -\frac{1}{R_N(C_N + C_P)} V_N - \frac{1}{R_P(C_N + C_P)} V_P + \frac{1}{C_N + C_P} I_N - \frac{C_P}{C_N + C_P} \dot{V}_B \\
&= -\left(\frac{1}{R_N} + \frac{1}{R} + \frac{1}{R_P}\right) \frac{1}{C_N + C_P} V_N + \frac{1}{R(C_N + C_P)} V_G - \frac{1}{R_P(C_N + C_P)} V_B \\
&\quad - \frac{C_P}{C_N + C_P} \dot{V}_B
\end{aligned} \tag{3}
$$

Let us define the parametric vector as follows:

$$
\begin{aligned}
\theta^T &= \left[\frac{1}{C_N + C_P}\left(\frac{1}{R} + \frac{1}{R_N} + \frac{1}{R_P}\right) \quad \frac{1}{R(C_N + C_P)} \quad \frac{1}{R_P(C_N + C_P)} \quad \frac{C_P}{C_N + C_P} \right] \\
&= \begin{bmatrix} \theta_1 & \theta_2 & \theta_3 & \theta_4 \end{bmatrix}
\end{aligned} \tag{4}
$$

and the variable vector as:

$$X^T = \begin{bmatrix} -V_N & V_G & -V_B & -\dot{V}_B \end{bmatrix} \tag{5}$$

such that the dynamics of the insulation monitoring system are formulated as follows:

$$\dot{V}_N = X^T \theta, \tag{6}$$

where the parametric vector includes all the resistance and capacitance values that must be known and the variable vector is composed of the variables that can be evaluated from all the measurements in the system, i.e., V_G, V_N, and V_P.

4. Proof of adaptive algorithm

If we suppose all the actual parameter values and the voltage V_N are unknown, we can write the dynamic model in an estimated formation as follows:

$$\dot{\widehat{V}}_N = \left[-\widehat{V}_N V_G - V_B - \dot{V}_B \right] \widehat{\theta} + u, \tag{7}$$

where $\widehat{Y}$ denotes the estimation of Y, and u is one part of the adaptation law that lets all the estimated values approach their true values, i.e., $\lim_{t \to \infty} \left| \widehat{V}_N(t) - V_N(t) \right| < \delta$ and $\lim_{t \to \infty} \left\| \widehat{\theta}(t) - \theta \right\| < \varepsilon$. We define the estimated error for V_N and the parametric vector as $e = V_N - \widehat{V}_N$ and $\widetilde{\theta} = \theta - \widehat{\theta}$, respectively. If we differentiate the estimated error, we have:

$$\dot{e} = \dot{V}_N - \dot{\widehat{V}}_N = \left[-\widehat{V}_N V_G - V_B - \dot{V}_B \right] \widetilde{\theta} - \theta_1 e - u. \tag{8}$$

Invoking the Lyapunov stability criteria shows that the positive-definite function:

$$S = e^2 + \widetilde{\theta}^T \Sigma \widetilde{\theta} \tag{9}$$

will approach zero for the negative semi-definite of its derivative; that is:

$$\dot{S} = \dot{e}e + \dot{\widetilde{\theta}}^T \Sigma \widetilde{\theta} = \left[-\widehat{V}_N V_G - V_B - \dot{V}_B \right] e\widetilde{\theta} - \theta_1 e^2 - ue - \dot{\widehat{\theta}}^T \Sigma \widetilde{\theta}$$

$$= -(\theta_1 + \lambda)e^2 + \left(\left[-\widehat{V}_N V_G - V_B - \dot{V}_B \right] e - \dot{\widehat{\theta}}^T \Sigma^{1/2} \right) \Sigma^{1/2} \widetilde{\theta} \tag{10}$$

$$= -(\theta_1 + \lambda)e^2 < 0,$$

provided that the adaptation law is as follows:

$$\dot{\widehat{\theta}} = \Sigma^{-1/2} \begin{bmatrix} -\widehat{V}_N e \\ V_G e \\ -V_B e \\ -\dot{V}_B e \end{bmatrix}, u = \lambda e^2, \text{ and } \lambda > 0, \tag{11}$$

where Σ could be a positive diagonal matrix for design simplicity. We can compute the insulation resistance as follows:

$$\widehat{R}_P = \frac{\widehat{\theta}_2}{\widehat{\theta}_3} R \text{ and } \widehat{R}_N = \frac{1}{\left(\frac{\widehat{\theta}_1}{\widehat{\theta}_2} - 1 \right) \frac{1}{R} - \frac{1}{\widehat{R}_P}}. \tag{12}$$

Figure 5 shows a calculation flowchart for estimating the insulation resistance. A detailed description of the process is as follows:

i. Start the online estimation at time t_0. The initial values of the estimated insulation resistance can be updated with the latest value in memory for faster convergence.

ii. The voltage values are acquired from the measured V_g, V_n, and V_p values.

iii. The estimated voltage error is computed by Eq. (7) together with the updated parameters, where the initial value of the estimated V_n can be identical to the measurement.

iv. Based on the measured voltage data and estimated V_n, the adaptive algorithm given in Eq. (11) updates the parameter. The updated parameters are sent to the previous and following steps.

v. The insulation resistances are calculated by Eq. (12) based on the updated parameters. The minimum value is used to check whether it is under the predetermined threshold. If so, it is shown in the indicator.

vi. The waiting time required for the parameters' convergence is calculated and T_m is empirically set up to avoid misjudgment.

vii. Either the insulation resistance or an alert message is displayed, depending on whether it is below the mandatory threshold.

viii. For continuous online monitoring, once started, this flow is an infinite loop.

5. Simulation and experimental results

To verify the proposed algorithm, for simplicity, we assumed a scenario in which an electric vehicle is driven on the road such that the battery and AC line voltages are $V_b = 350$ V and $V_a = 0$ V, respectively. We set the initial insulation resistances at the positive and negative terminals to earth to be within the safety level, i.e., $R_p(t = 0 \text{ s}) = 600$ kΩ and $R_n(t = 0 \text{ s}) = 500$ kΩ, respectively. After 60 s, we degraded $R_n(t = 60 \text{ s})$ to 100 kΩ, and after 120 s, we did the same for $R_p(t = 120 \text{ s})$. To precisely characterize the electrical behavior of the equivalent circuit shown in **Figure 4**, we considered their parallel parasitic capacitances to be invariant at $C_p = 0.3$ uF and $C_n = 0.2$ uF. For the insulation resistance monitor, we selected the resistor R to be 20 kΩ, and we initially guessed the estimated values for R_p/R_n to be 350 kΩ/100 kΩ.

We constructed the circuit model and the estimation algorithm using Simulink software. The simulation estimation results for R_p and R_n are depicted in **Figures 6** and **7**, respectively. These figures show that the estimated R_p approaches the actual value within 20 s, but the estimated R_n converges to the actual value after 50 s. The relative error between actual and estimated values are both less than 1%. With respect to two degradation cases that sequentially occur on the negative and positive terminals, we found that either of the degradations would yield some fluctuation in the estimated value on the opposite side, particularly a case in which the degradation occurs on the positive terminal. As a consequence, it requires more time for convergence, i.e., 20 and 240 s for the degradations occurring on the negative and positive
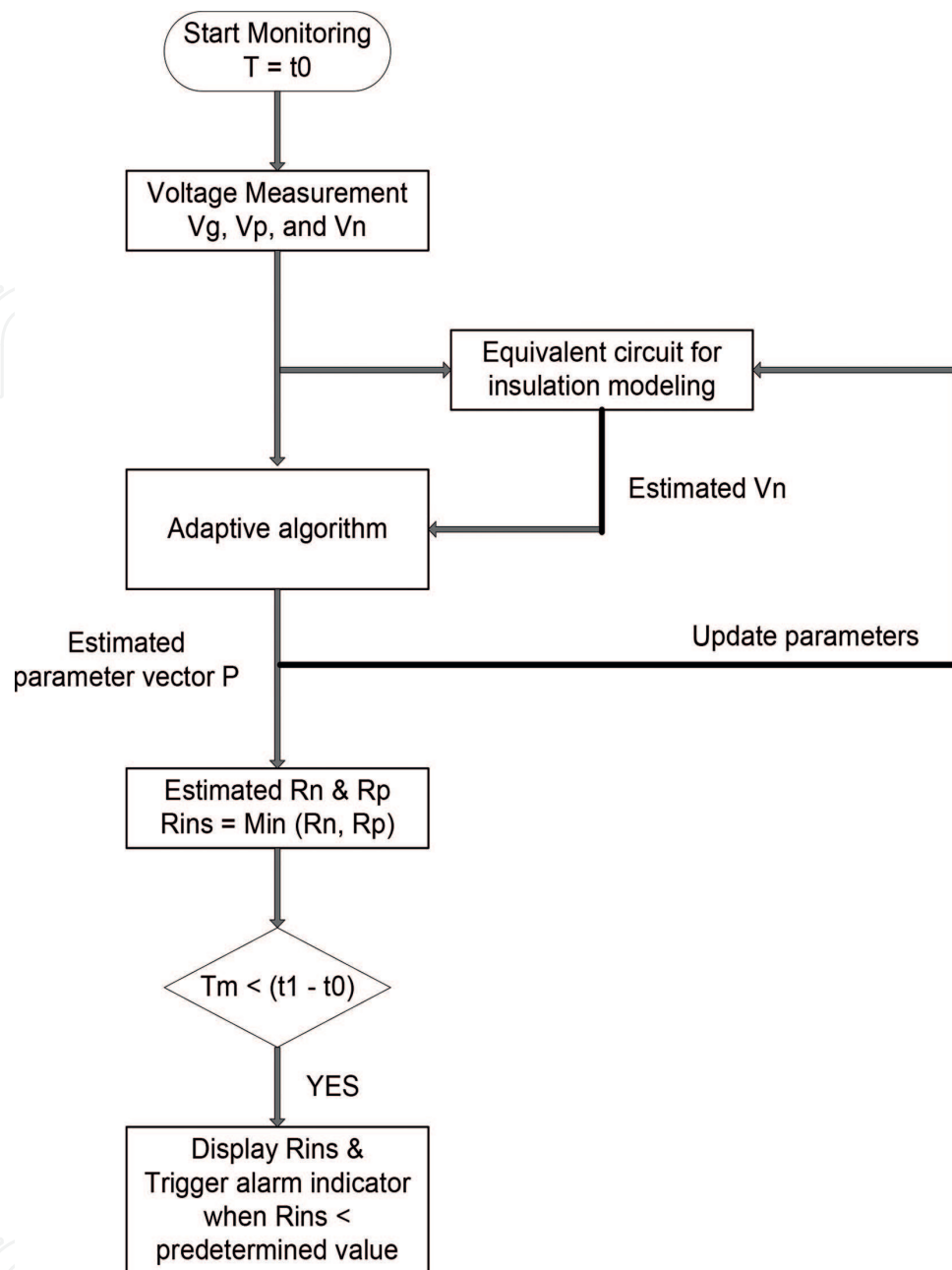
Figure 5. Flowchart for online parameter estimation.

sides, respectively. This is because the proposed circuit is directly connected to the negative terminal, which makes it more sensitive to voltage variations across the negative terminal and chassis ground. In other words, the high battery voltage V_b would attenuate the excitation signal coming from the negative side. Nevertheless, the simulation verifies that the proposed algorithm can estimate the actual insulation resistance and monitor its variation in the circuit model, while also considering the parasitic capacitance, as shown in **Figure 4**. To avoid false alarms due to ground fault detection when using this method, fault counting is necessary over a period of time.
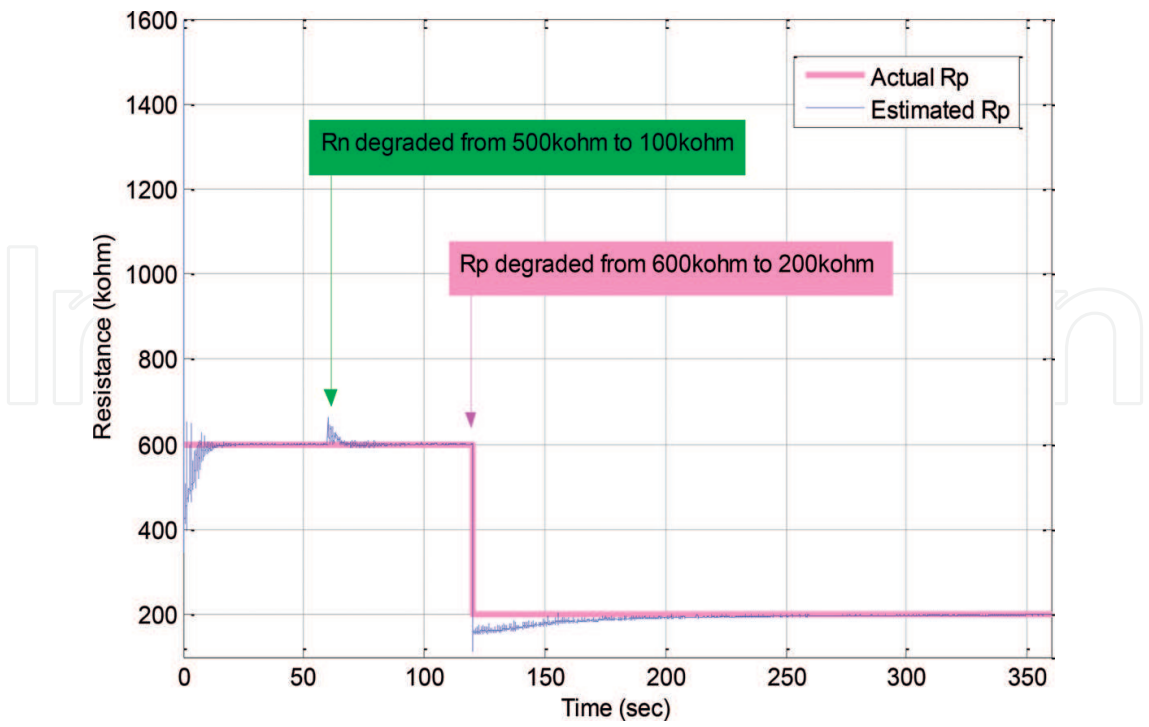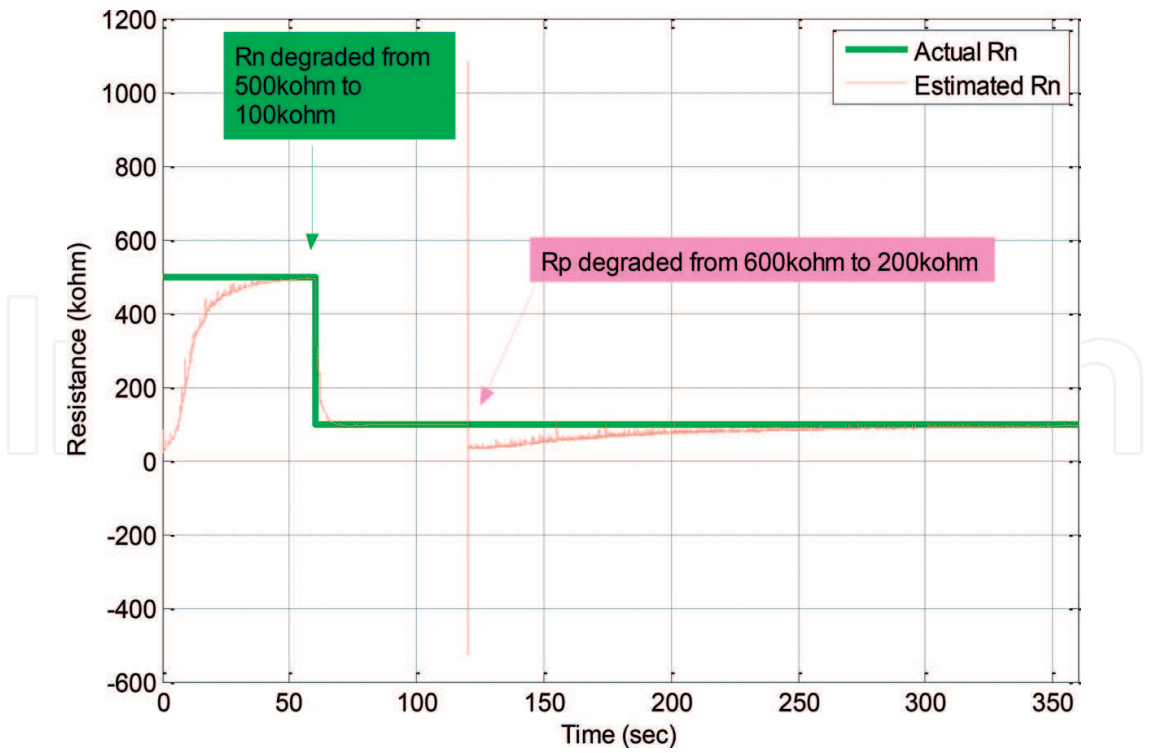
Figure 6. Estimation of R_p.

Figure 7. Estimation of R_n.

To simply validate the proposed algorithm in the laboratory, we connected a variable resistor to the proposed circuit to form a left-hand side loop of the circuit shown in **Figure 4**, in which the resistance, as represented by R_n, is the value to be estimated. Due to the simplicity of the single loop circuit, using Kirchhoff's current law, R_n can be evaluated in a straightforward manner, as follows:
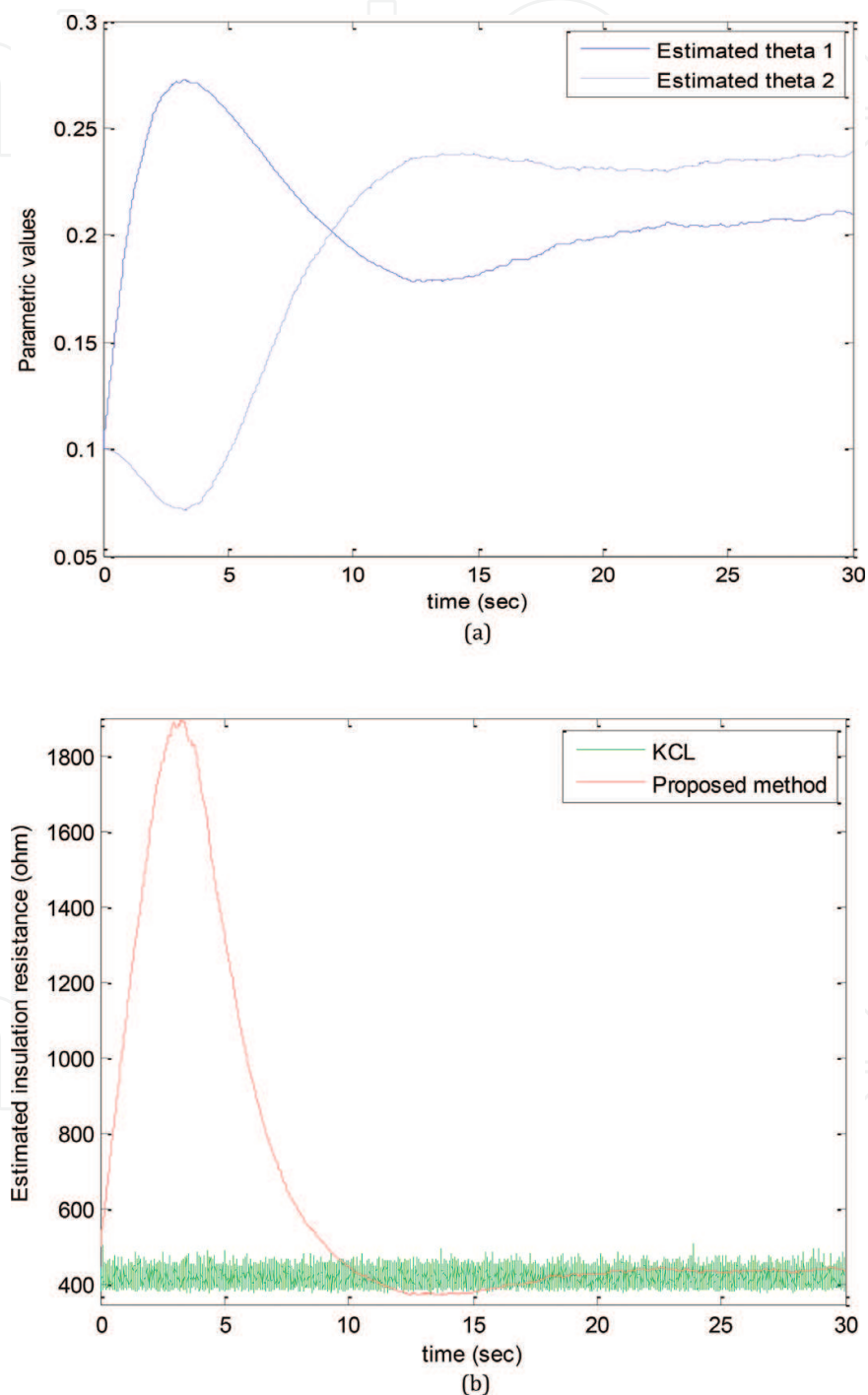

Figure 8. Experimental results. (a) Estimated parameters $\widehat{\theta}_1$ and $\widehat{\theta}_2$. (b) Estimated resistances of the two models.

$$R_n = \frac{R}{\frac{V_G}{V_N} - 1} \qquad (13)$$

On the other hand, we modify the estimated model to yield:

$$R_n = \frac{\widehat{\theta}_1}{\widehat{\theta}_2} R. \qquad (14)$$

The experimental results are shown in **Figure 8**. In **Figure 8(a)**, the two estimated parameters converge after 25 s. In **Figure 8(b)**, we depict the online estimated resistances based on the straight evaluation of Eq. (8) and the proposed method in Eq. (9). It is realized that the estimated value by using the straight evaluation varies roughly 10% between its maximum and minimum values. This may be due to either measurement noise or the dynamic uncertainty of the parasitic capacitance. However, the proposed method shows a steadier and more exact estimation after the convergence of the model parameters.

6. Conclusions

In this chapter, to improve existing techniques for enhancing the safety and reliability of high-voltage systems, we proposed a new insulation resistance online monitoring method for EV high-voltage DC lines, which takes into account the parasitic capacitance effect. The estimation scheme based on an adaptive control algorithm guarantees the asymptotical convergence of the parameters in the circuit model. Hence, as demonstrated in our simulation and experimental results, this method can steadily and accurately track the insulation resistance even when the parasitic capacitance is unknown. Due to the simplicity of the proposed algorithm and circuit, they can be easily implemented via electronic circuit design in real cases. According to the results, the estimated R_p and R_n converge to the actual value in 50 s. The relative error between actual and estimated values are both less than 1%. With respect to two degradation cases that sequentially occur on the negative and positive terminals, it requires more time for convergence, i.e., 20 and 240 s for the degradations occurring on the negative and positive sides, respectively.

Nomenclature

AC   alternating current

BMS   battery management system

DC   direct current

DC/DC   conversion of a DC source from one voltage level to another

ECM   equivalent-circuit model

EV   electric vehicle

MCU   micro-control unit

PRBS   pseudo random binary sequence

PWM   pulse-width modulation

SoC   state of charge

SoH   state of health

UPS   uninterrupted power supply

Author details

Yi-Hsien Chiang and Wu-Yang Sean*

*Address all correspondence to: wuyangsean@gmail.com

Department of Environmental Engineering, Chung Yuan Christian University, Taiwan

References

[1] Stimper K. Physical fundamentals of insulation design for low-voltage equipment. IEEE Transactions on Electrical Insulation. 1990;**25**(6):1097-1103

[2] Baldwin T, Renovich F, Saunders LF. Direction ground-fault indicator for high-resistance grounded systems. IEEE Transactions on Industry Applications. 2003;**39**(2):325-332

[3] Huang H-H, Quan C, Huang J. Development of distributed DC grounding detecting system based on differential current detecting method. Journal of Electronic Measurement and Instrument. 2009;**23**(11):8

[4] Li L-W, Liu X-F, Liu B. Distributed on-line grounding monitoring system for DC system based on field bus. Electric Power Automation Equipment. 2006;**26**(12):55-58

[5] Guo H-Y, Jiang J-C, Wen J-P, Wang J-Y. New method of insulation detection for electrical vehicle. Journal of Electronic Measurement and Instrument. 2011;**25**(3):253-257

[6] Kota O, Balasubramanian G. High voltage safety concepts for power electronic units. SAE Technical Paper; 2013

[7] Li J-X, Fan Y-Q, Jiang J-C, Chen H. An approach to on-line monitoring on insulation resistance in electric vehicle. Automotive Engineering. 2006;**28**(10):884-887

[8] Li L, Jiang J-C. Research on battery insulation detection for electric vehicle. Electronic Measurement Technology. 2009;**32**(2):76-78

[9]   Pan L, Jiang J, Li J. Development of intelligent passive grounding detection device for electric vehicle. Electrical Drive Automation. 2003;**25**(4):47-48

[10] Wu Z-J, Wang L-F. A novel insulation resistance monitoring device for hybrid electric vehicle. In: IEEE Conference on Vehicle Power and Propulsion (VPPC); 2008

[11] Morimoto N. Ground-fault resistance measurement circuit and ground-fault detection circuit. US Patent No. 7560935B2

[12] Onnerud P, Linna JR, Warner J, Souza C. Safety and performance optimized controls for large scale electric vehicle battery systems. US Patent No. 20110049977A1

[13] Chiang Y-H, Sean W-Y, Huang C-Y, Hsieh L-HC. Adaptive control for estimating insulation resistance of high-voltage battery system in electric vehicles. Environmental Progress & Sustainable Energy. 2017;**36**(6):1882-1887

[14] Sottile TN, Tripathi AK. Best practices for implementing high-resistance grounding in mine power systems. IEEE Transactions on Industry Applications. 2015;**51**(6):5254-5260. DOI: 10.1109/TIA.2015.2420632